Available online at www.sciencedirect.com
ScienceDirect
Trans. Nonferrous Met. Soc. China 35(2025) 2074−2090
Transactions of Nonferrous Metals Society of China
www.tnmsc.cn

Efficient removal of impurity Bi element from scrap brass by compound-separation method

Fei-ran JIANG[1], Chuan-rong JIAO[1], Li-juan WANG[1], Rui-lin WU[1], Yan-bin JIANG[1,2,3], Qian LEI[2], Meng WANG[1], Zhu XIAO[1,3], Zhou LI[1,2,3]

1. School of Materials Science and Engineering, Central South University, Changsha 410083, China;
2. State Key Laboratory of Powder Metallurgy, Central South University, Changsha 410083, China;
3. Shanxi Key Laboratory of Copper-based New Materials, Yuncheng 044000, China

Received 11 May 2024; accepted 21 October 2024

Abstract: Highly efficient removal of impurity Bi element from scrap brass can facilitate the recycling process of brass. The effects of melting temperature, holding time and Mg−Ca alloy content on the removal effect of impurity Bi element were investigated by compound-separation method. The mechanism of the compound-separation method was revealed for removing the Bi element from a thermodynamic point of view. The results showed that the Bi content was decreased from 1.95 wt.% to 0.178 wt.% at the optimum process parameters of melting temperature of 980 °C, holding time of 20 min, and Mg−Ca alloy content of 6 wt.%, achieving a removal rate of 90.9%. A small amount of Ca−Bi compound remained in the brass matrix after refining. NaF flux can effectively wet and adsorb Ca−Bi compounds due to its low viscosity and the function of lowering the surface tension, which facilitate the agglomeration and flotation of Ca−Bi compounds to the melt surface, thereby ensuring the sufficient removal of Bi element.
Key words: scrap brass; Bi-rich phase; Mg−Ca alloying; compound-separation method

1 Introduction

With the sustained and rapid development of the global copper processing industry, the world's demand for copper resources is increasing. Currently, China ranks the first in the world in terms of refined copper production and consumption. However, China's copper ore reserves are small and account for only 5.53% of the world's reserves, which is a typical copper-poor country [1]. According to the survey [2−4], China's refined copper production was approximately 11.06×10^6 t, but its consumption of refined copper was 14.15×10^6 t in 2022. The estimated demand for copper production over the next 2035 will be about 50 times more than the supply. The significant demand for copper in China's economic development and the remarkable contradiction of the shortage of copper resources have put forward a more urgent demand for the development of copper recycling technology.

Copper metal itself has good recyclability and can be repeatedly reused. For this reason, focusing on the development of secondary resource utilization of recycled copper can not only alleviate the pressure of the shortage of copper resources and improve the utilization rate of scrap copper resources but also reduce energy consumption, minimize environmental pollution, and boost the economic benefits of copper processing industries [4−6].

As an important raw material in scrap copper, the recycling of scrap brass plays a crucial role in the green and sustainable development of the

Corresponding author: Yan-bin JIANG, Tel: +86-13466312126, E-mail: jiangyanbin@tsinghua.org.cn
https://doi.org/10.1016/S1003-6326(25)66802-6

non-ferrous metal industry. There is a wide variety of impurity elements in the scrap brass [7,8], and the common impurity elements include Pb, Bi, Sn, Al, Fe, Ni, etc. The addition of appropriate alloying elements generally enhances the properties of brass alloys to a certain extent. Otherwise, it may deteriorate the comprehensive performance of brass alloys. Bi element has a low melting point (271.4 °C) and its solid solubility in copper does not exceed 0.03 wt.%. It often exists in elemental form and is distributed along grain or phase boundaries. Bi has good wettability with the copper alloy matrix, and its uniform distribution in brass alloys is beneficial to the enhancement of brass's machinability. However, excessive Bi content is distributed at the interface of α-phase and β-phase in the form of a reticulated thin film, which makes the alloy develop a serious tendency to thermal brittle cracking and greatly reduces its hot working properties.

Currently, direct separation and removal of impurity elements from scrap brass is the most dominant method. There are various methods for separating and removing impurities from scrap brass, which can be specifically subdivided into the following methods: dilution degradation [9,10], conventional flux refining [11−14], modifier refining and modification [15−18], vacuum-distillation [19], compound separation [20−22], pulsed current melt treatment technology, and gravity field separation [23−27].

Compound separation is one of the most widely applied methods for melt purification. This method involves adding an alloying element that can interact with impurity elements, forming intermediate compounds that are subsequently adsorbed and captured by the flux into the slag, thus accomplishing the separation and removal of impurity elements. It offers the advantages of simplicity, ease of operation, and high feasibility. The compound-separation method has been successfully applied to the separation of Pb element from brass melt. NAKANO et al [22] added Ca element to bronze and brass with high Pb content, forming high melting point, low-density inter-metallic compounds that floated to the surface of the melt, which were ultimately skimmed and removed by slagging. Furthermore, LU et al [28] investigated the mechanism of Bi removal by Ca and Mg, revealing that bismuthide in the slag mainly existed in the form of $Ca_3Mg_7Bi_8$, i.e. Ca_3Bi_2, CaBi, $CaBi_3$, Mg_3Bi_2, and Mg solid solution, which provides a basis for the separation of Bi element in the scrap brass.

The physical and chemical properties of Pb and Bi elements are similar, and both of them are impurity elements that are difficult to remove from scrap brass. However, this method has not yet elucidated the separation effect and removal mechanism of the Bi element in the scrap brass, and there is a lack of corresponding systematic research.

To promote the efficient recycling and reuse of scrap Bi brass, in this work, Mg−Ca alloy and NaF flux were used as refining agents, and the influences of melting temperature, holding time, and Mg−Ca alloy content on the removal effect of the impurity Bi element were investigated by compound-separation method, revealing the mechanism of synergistic Bi removal by alloying elements and flux from a thermodynamic point of view. This work provides a reference for efficiently removing Bi element from scrap Bi brass using the compound-separation method.

2 Experimental

2.1 Experimental procedure

The designed Cu−38Zn−2Bi (wt.%) brass alloy was prepared in an intermediate-frequency induction furnace using electrolytic copper (99.95 wt.%), pure zinc (99.95 wt.%), and pure bismuth (99.95 wt.%) as the raw materials and cast into a graphite mold. The actual chemical composition of the brass alloy is shown in Table 1. The actual content of the Bi element was 1.95 wt.%, which was basically close to the design composition.

Firstly, about 1 kg of scrap brass per furnace was used as raw material. The scrap brass was placed in the graphite crucible. To avoid the oxidative burnout of the Zn element, $Na_2B_4O_7$ and Na_2CO_3 covering agents were added before melting, and the addition of covering agent accounts for 0.8 wt.% relative to copper melt. After addition, the temperature was raised to ensure that the raw materials were completely melted and the melt was stirred sufficiently, then the temperature parameter was adjusted to keep the melt at the target temperature. Secondly, Mg−Ca alloy wrapped in copper foil was added, stirred, and held for a certain

period. Finally, NaF flux wrapped by copper foil was added and held for 10 min, and then skimming, casting, and sampling were carried out. The addition of NaF flux was 2 wt.%. The schematic diagram of the experimental process is shown in Fig. 1.

Table 1 Chemical composition of scrap brass raw materials (wt.%)

Zn	Bi	Cu
38.50	1.95	Bal.

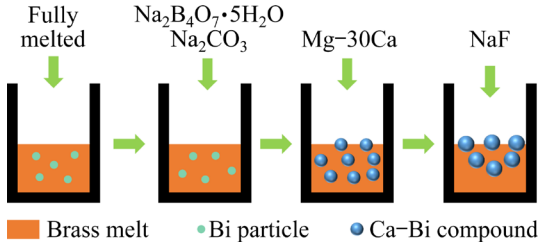

Fig. 1 Schematic diagram of experiment procedure

The refining process parameters in experiments were as follows: melting temperatures of 980, 1000, 1020, and 1040 °C; holding time of 0, 10, 20, 30, and 40 min; Mg−Ca alloy content accounted for 1 wt.%, 2 wt.%, 4 wt.%, 6 wt.%, and 8 wt.% relative to scrap brass, respectively.

2.2 Materials characterization

The content of Bi element in brass alloys was determined by inductively coupled plasma emission spectrometry (ICP-OES, SPECTRO BLUE SOP). Brass samples of 10 mm × 10 mm × 3 mm were cut using electric arc spark wire cutting and their surfaces were polished by SiC sandpaper. Then, the microstructure of the brass samples was characterized by using a scanning electron microscope (SEM, TESCAN MIRA4 LMH) equipped with an energy dispersive spectrometer (EDS, Ultim Max 40). The phase composition of brass alloys and slag were analyzed by X-ray diffraction (XRD, Smartlab SE), in which the scanning angle ranged from 10° to 90° with a scanning rate of 5 (°)/min.

3 Results and discussion

3.1 Microstructure of as-cast bismuth brass

Figure 2(a) shows the XRD pattern of as-cast

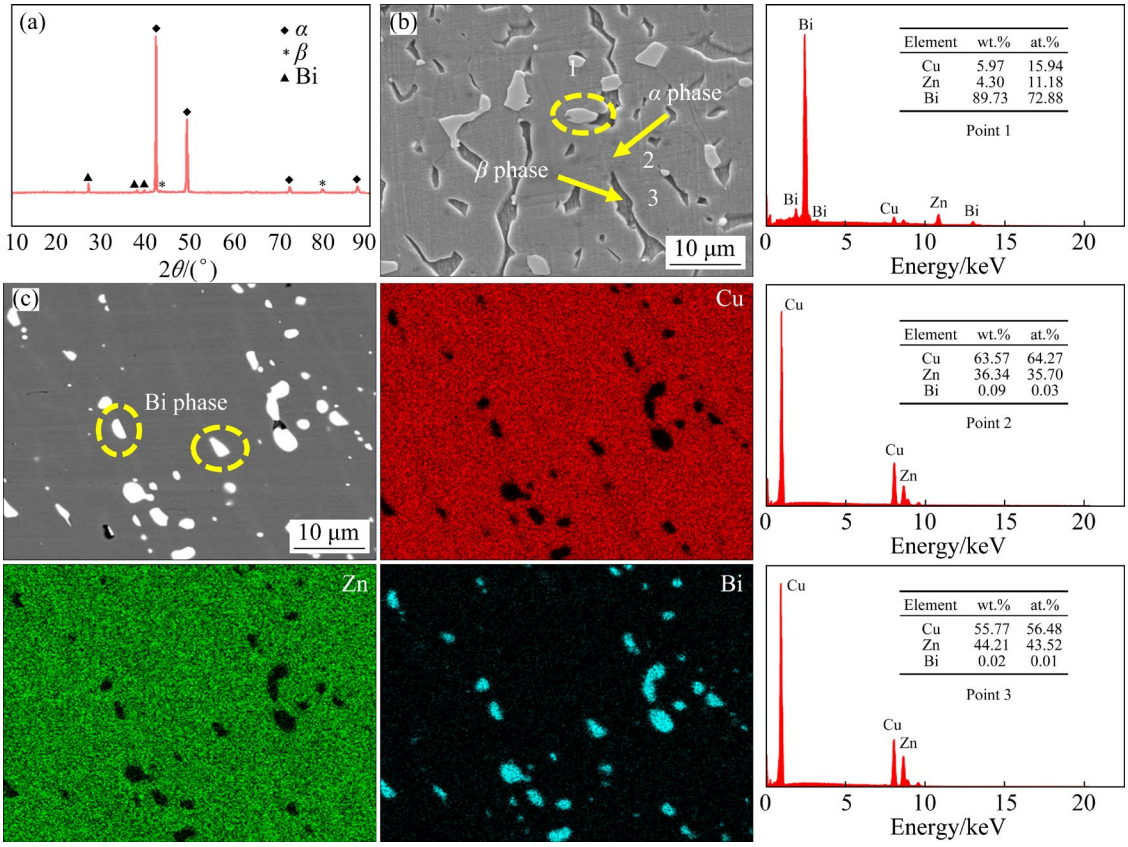

Fig. 2 Microstructure of as-cast bismuth brass: (a) XRD pattern; (b, c) SEM−EDS analysis results

bismuth brass. It can be seen that the scrap brass consists of three phases, which are α-phase ($Cu_{0.64}Zn_{0.36}$), β-phase (CuZn), and Bi-phase. Figures 2(b) and (c) show the SEM−EDS results of as-cast bismuth brass. According to the phase diagram of the Cu−Zn binary alloy, the brass alloy with 38 wt.% Zn content consisted of α-phase ($Cu_{0.64}Zn_{0.36}$) and β-phase (CuZn), as shown in Fig. 2(b). Combined with the EDS mapping results (Fig. 2(c)), it was observed that the phase in the white region was a Bi-rich phase, and the average particle size of the Bi-phase was approximately 1.72 μm.

3.2 Effect of reaction temperature

The melting temperature is crucial for the occurrence of the melt reaction. The melting temperatures were determined to be 980, 1000, 1020, and 1040 °C, with Mg−Ca alloy content of 6 wt.%, and the holding time of 30 min based on the melting point of brass alloy, as shown in Fig. 3.

From Fig. 3(a), it can be found that with the increase of melting temperature, the content of the Bi element exhibited a tendency to increase and then decrease. When the melting temperature was 980 °C, the content of the Bi element was 0.39 wt.%. As the temperature increased to 1000 °C, the oxidation of Zn, Mg, and Ca elements during the melting process led to a relative increase in the content of Bi element. Therefore, the Bi content rose to 0.65 wt.%. However, as the temperature was further increased to 1040 °C, the Bi content was decreased from 0.65 wt.% to 0.47 wt.%. Accordingly, the removal rate of the Bi element showed a tendency to decrease first and then increase. The removal rate of the Bi element decreased from 79.8% to 66.8% by varying the melting temperature from 980 to 1000 °C. Subsequently, when the melting temperature was increased to 1040 °C, the removal rate of Bi element increased to 75.9%. The Zn content gradually decreased with increasing temperature and was lower compared with the initial state content, which is attributed to the easy oxidative burnout of the Zn element (Fig. 3(b)). The Mg content ranged from 1.50 wt.% to 3.35 wt.% and the Ca content ranged from 0.18 wt.% to 0.33 wt.%, as shown in Figs. 3(c, d). This result may be attributed to the fact that the Mg and Ca elements are both more reactive and have different degrees of burnout during high-temperature melting.

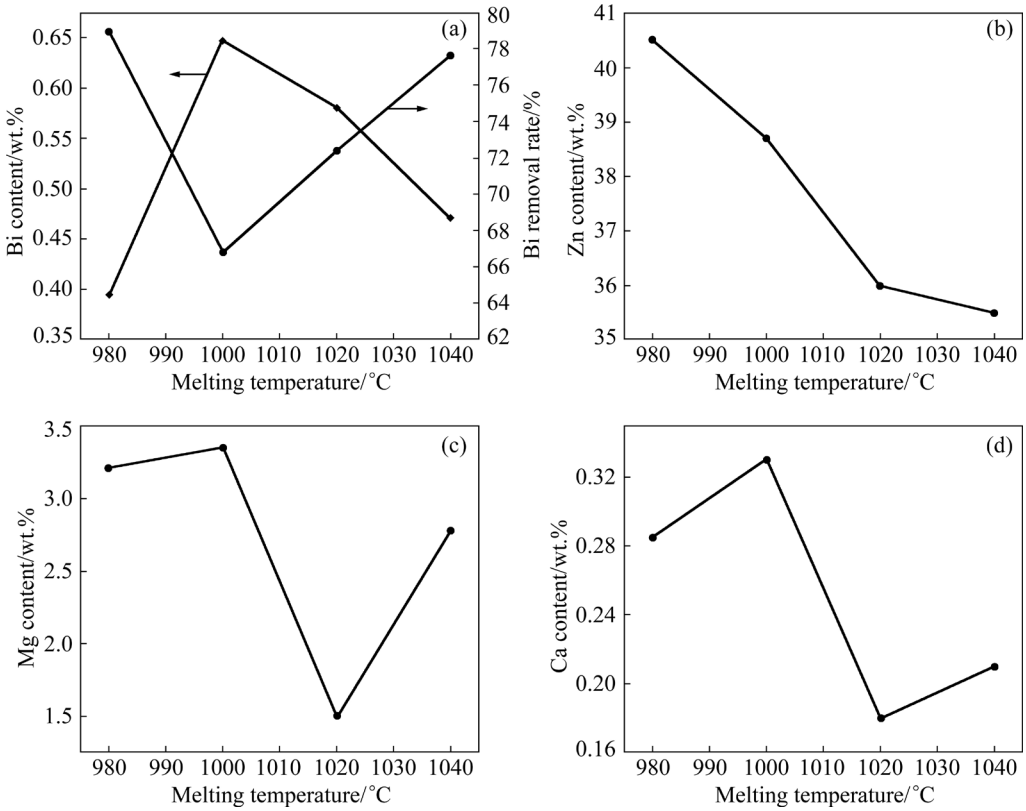

Fig. 3 Chemical compositions of brass samples refined at different temperatures: (a) Bi; (b) Zn; (c) Mg; (d) Ca

Based on the above experimental results, optimal melting temperature was determined to be 980 °C.

Figure 4 displays the SEM−BSE images of as-cast and refined brass samples at different melting temperatures. Compared to the unrefined state, it can be observed that the Bi-rich phase was mainly aggregated and distributed in the darker region after refining. The number of Bi-rich phase particles in the refined samples showed a tendency to decrease and then slightly increase with the increase of temperature. After refining at 980 and 1000 °C, the

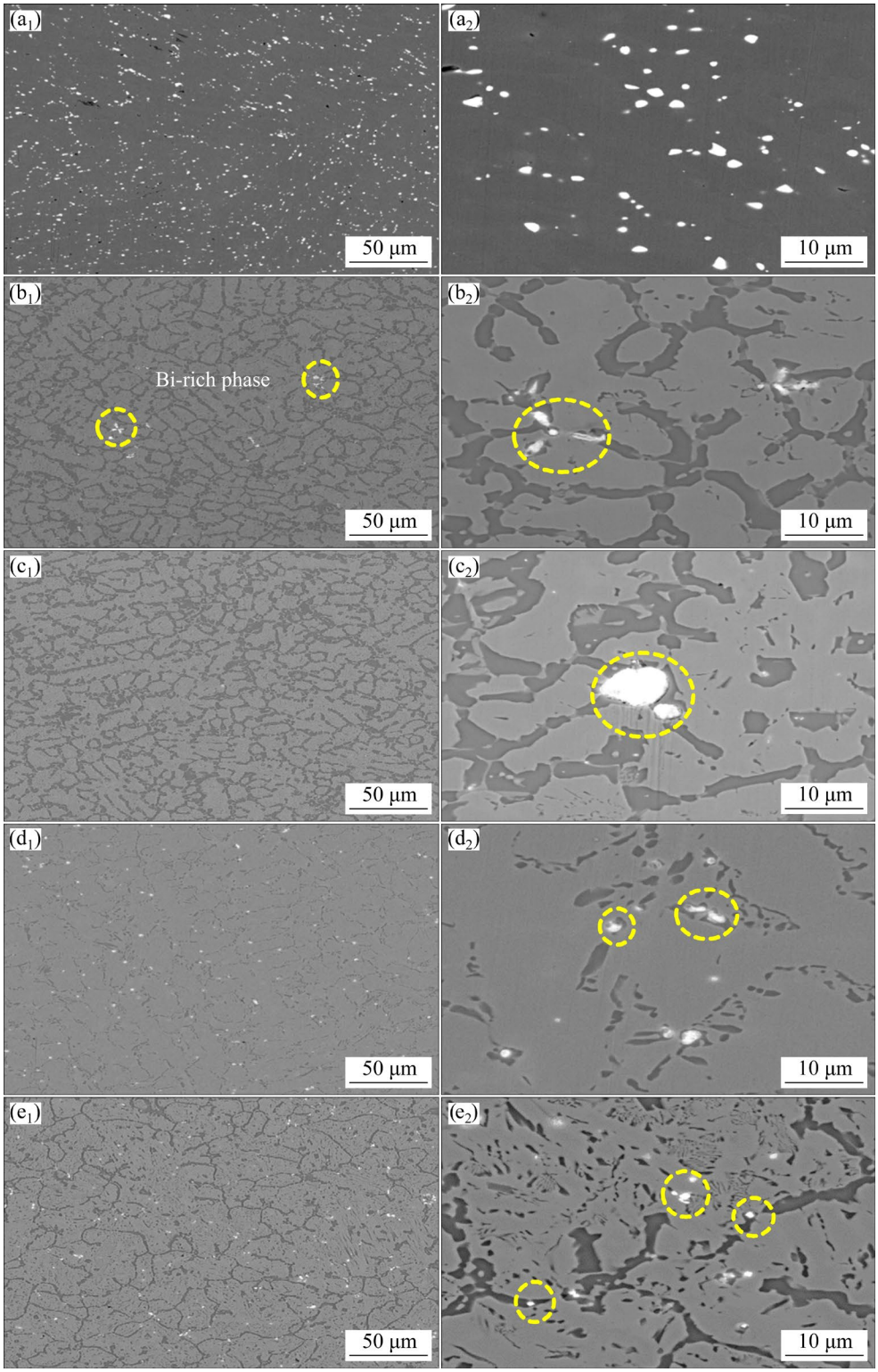

Fig. 4 SEM−BSE images of as-cast and refined brass samples at different temperatures: (a_1, a_2) As-cast; (b_1, b_2) 980 °C; (c_1, c_2) 1000 °C; (d_1, d_2) 1020 °C; (e_1, e_2) 1040 °C

number of Bi-rich phase particles decreased dramatically, and only a very small amount of Bi-rich phase was observed in the matrix, indicating that the removal effect of Bi element was better at these temperatures. As the temperature was further increased to 1020 and 1040 °C, the number of Bi-rich phase particles in the matrix increased instead, suggesting a slight decrease in the removal effect.

In order to further explore the elemental composition of the Bi-rich phase, a brass sample refined at 980 °C for 30 min was selected as a representative for mapping analysis, as shown in Fig. 5. The white particles distributed in the dark region showed partial overlapping of Ca and Bi elements, indicating that the white particles consisted of Ca−Bi compound and Bi-phase. This also suggested that Ca may react with the impurity element Bi. This reaction will allow the Bi-phase to be distributed in the Cu matrix in the form of an intermetallic compound. In addition, the Mg element was primarily distributed in the dark region, along the grain boundary, and mainly inside the β-phase. These results were in agreement with other researches [29,30].

3.3 Effect of holding time

The holding time typically affects whether the chemical reaction sufficiently occurred. Appropriate prolonging the holding time ensures that Ca reacts adequately with the Bi element. For this purpose, the melting temperature was set to be 980 °C, the holding time was 0, 10, 20, 30, and 40 min, and the Mg−Ca alloy content was 6 wt.%, as shown in Fig. 6.

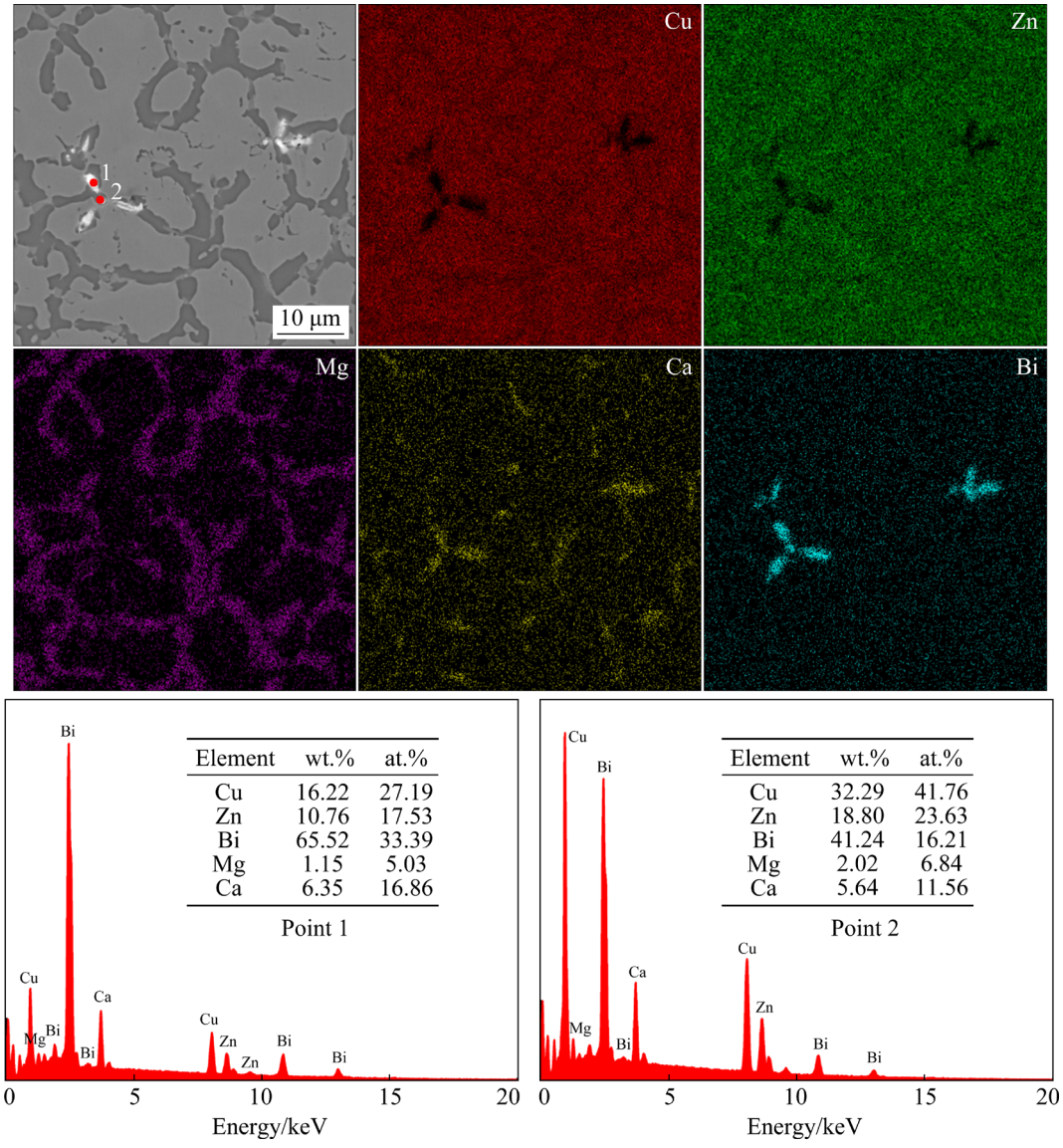

Fig. 5 SEM−EDS analysis results of brass sample refined at 980 °C for 30 min

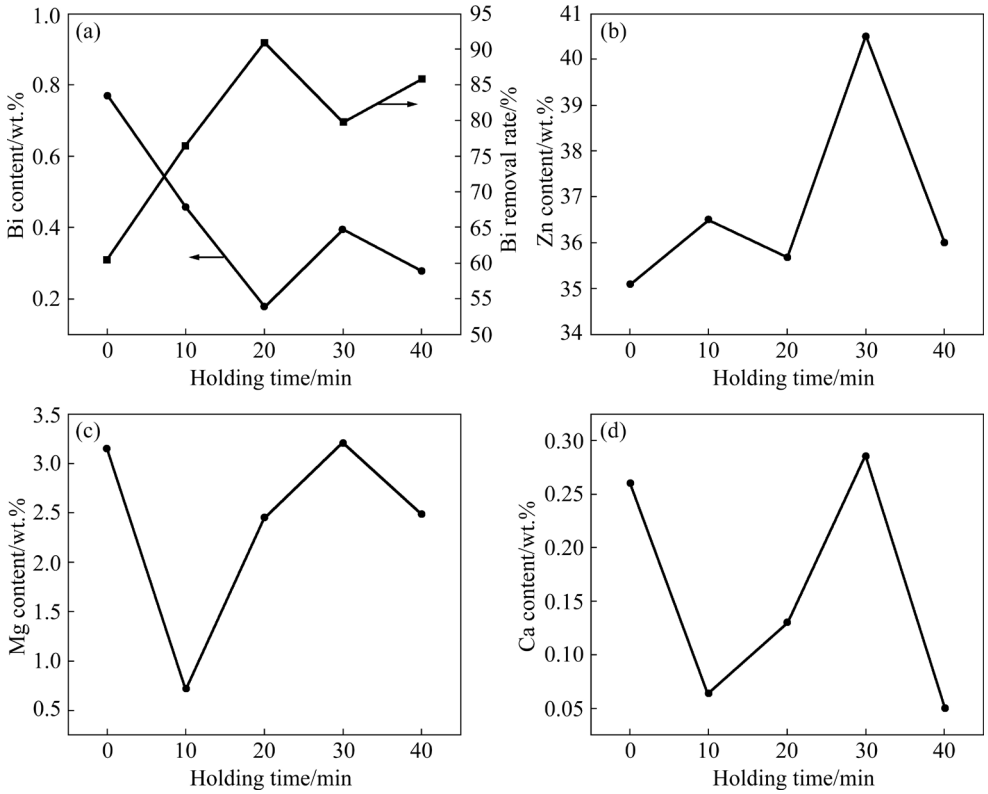

Fig. 6 Chemical compositions of brass samples refined for different holding time: (a) Bi; (b) Zn; (c) Mg; (d) Ca

It was found that with the extension of the holding time, the Bi content showed a trend of decreasing first, then increasing, and finally slightly decreasing. When the holding time was increased from 0 to 10 min, the Bi content decreased from 0.77 wt.% to 0.458 wt.%. With the prolongation of the holding time to 20 min, the Bi content was the lowest, with a value of 0.178 wt.%, and the corresponding removal rate reached up to 90.9%, which indicated that the reaction between Ca and Bi element at this time was more sufficient. However, with the further extension of the holding time to 30 min, the content of Bi element increased from 0.178 wt.% to 0.394 wt.%, and the impurity removal rate was 79.8%. This phenomenon can be attributed to the oxidation of Ca, Zn, and Mg elements. When the holding time was 40 min, the Bi content was slightly reduced to 0.277 wt.%, and the impurity removal rate was 85.8%. Therefore, the optimal holding time was determined to be 20 min. The Zn content was overall lower than that of the raw materials as the holding time varied. The Mg content ranged from 0.72 wt.% to 3.211 wt.% and the Ca content ranged from 0.0505 wt.% to 0.285 wt.%, as depicted in Figs. 6(b, c, d).

Figure 7 displays the SEM−BSE images of brass samples after refining for different holding time. As shown in Fig. 7, a certain number of Bi-rich phase particles can be observed in the brass matrix as the holding time was prolonged. Among them, the number and size of Bi-rich phase particles with a holding time of 0 min were larger. When the holding time was 10 min, the size of Bi-rich phase particles was smaller and the distribution of Bi-phase was more dispersed. The number of Bi-rich phase particles decreased slightly with the extension of the holding time to 20 and 30 min. When the holding time was 40 min, there was no obvious change in the number and size of the Bi-rich phase particles. In addition, the brass matrix after different holding time varied slightly. The difference was mainly due to the variation of Mg content. Combined with Fig. 6(c), when the holding time was 10 min, the content of the Mg element was only 0.72 wt.%, solidly dissolved in the brass matrix, and the dark concave region β-phase was narrow. As the Mg content in the brass matrix gradually increased, as shown in Figs. 7(a, c, d, e), the β-phase in the dark concave region gradually increased, especially in Figs. 7(a, d). The above results also indicated that the Mg element can promote the generation of the β-phase.

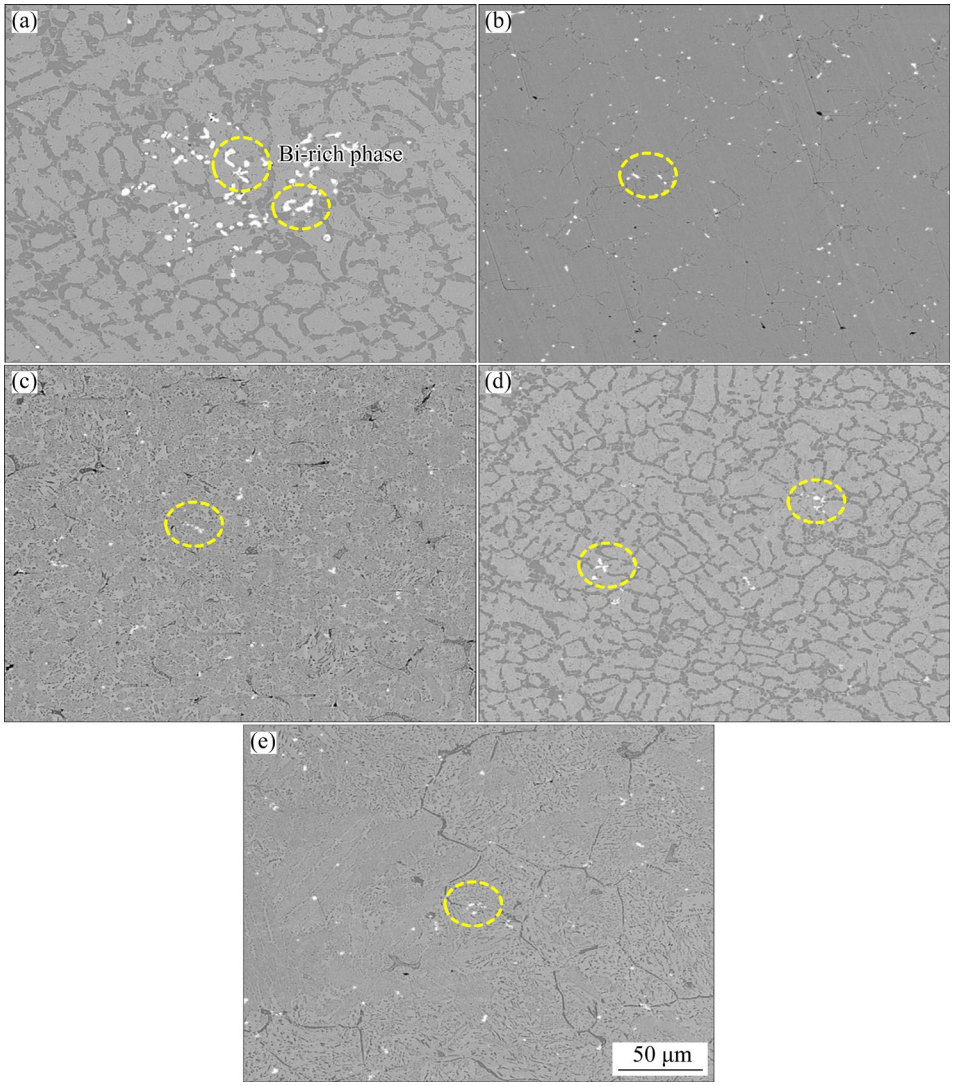

Fig. 7 SEM−BSE images of brass samples refined for different holding time: (a) 0 min; (b) 10 min; (c) 20 min; (d) 30 min; (e) 40 min

Figure 8 shows the SEM−EDS results of the brass sample after refining at 980 °C for 20 min. According to the mapping analysis results, the presence of the Ca element was observed in the corresponding region of the Bi element, indicating that the Bi-rich phase was composed of the Ca−Bi compound and Bi-phase. This result also suggested that Ca may react with the Bi element, thereby transforming the distribution morphology of the Bi-phase. In addition, it was noticed that the Bi-rich phase underwent an obvious agglomeration.

3.4 Effect of Mg−Ca alloy content

To investigate the effect of Mg−Ca alloy content on the removal effect of Bi element, the Mg−Ca content was set to be 1 wt.%, 2 wt.%, 4 wt.%, 6 wt.%, and 8 wt.%, respectively, with the melting temperature and the holding time set to be 980 °C and 20 min, respectively, as shown in Fig. 9.

The content of Bi element decreased gradually with the increase of Mg−Ca alloy content. Accordingly, the removal rate of Bi element increased with the increase of Mg−Ca alloy content. When the content of Mg−Ca alloy was 1%, the Bi content and impurity removal rate of the brass alloy were 1.38 wt.% and 29.2%, respectively. The content of the Bi element decreased more with the increase of Mg−Ca alloy content to 2%, and the Bi content and the removal rate were 0.635 wt.% and 67.4%, respectively. When the content of Mg−Ca alloy was 4 wt.%, the Bi content further decreased to 0.407 wt.% and the removal rate reached 79.1%. It was worth noting that there was no significant

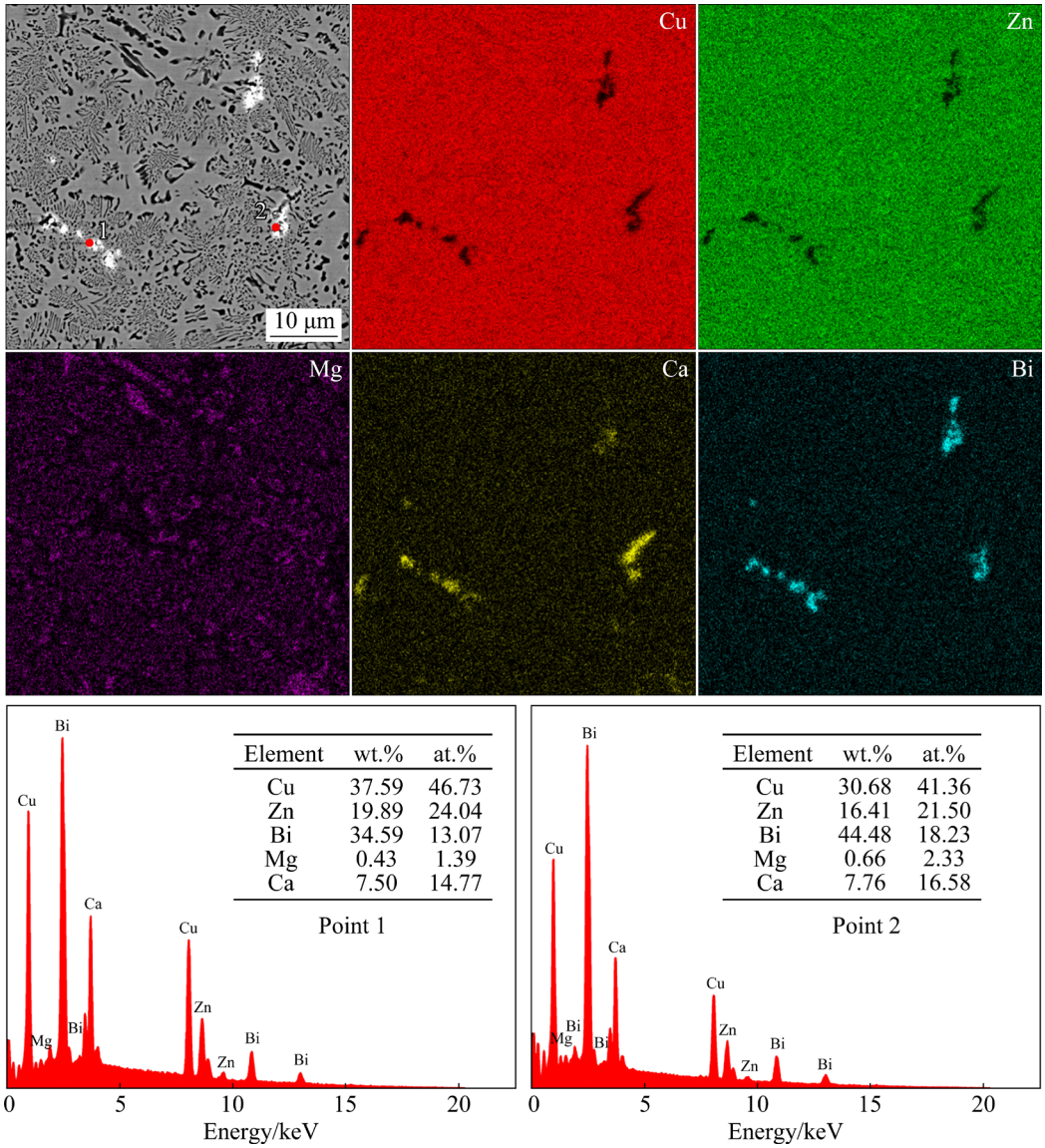

Fig. 8 SEM−EDS analysis results of brass sample refined at 980 °C for 20 min

difference in the Bi content as the Mg−Ca alloy content increased to 6 wt.% and 8 wt.%, with values of 0.178 wt.% and 0.171 wt.%, respectively. In terms of actual production cost, as revealed by the results, the optimal content of Mg−Ca alloy under the experimental conditions was 6 wt.%.

After refining, the Bi content and removal rate in the scrap brass were 0.178 wt.% and 90.9%, respectively. As the Mg−Ca alloy content increased from 2 wt.% to 8 wt.%, the Zn content gradually decreased, which was still lower compared to the initial state content, as illustrated in Fig. 9(b). The Mg and Ca contents gradually increased, with the Mg content ranging from 0.0008 wt.% to 4.01 wt.% and the Ca content ranging from 0.0012 wt.% to 0.53 wt.%, as shown in Figs. 9(c, d).

To investigate the elemental composition of the Bi-rich phase in the brass samples under the condition of different Mg−Ca alloy contents, the brass samples were analyzed for elemental distribution, as shown in Fig. 10. The results showed that the white phase was primarily a Bi-phase when the Mg−Ca alloy content was only 1 wt.%. As the Mg−Ca alloy content reached 2 wt.%, Mg and Bi elements were detected in the white phase, while Ca element was not detected, indicating that Mg formed the Mg−Bi compound with Bi element. When the Mg−Ca alloy content was 4 wt.% and 6 wt.%, Ca element was detected at the corresponding position of Bi element, as shown in Figs. 10(c, d), suggesting that the white phase was composed of the Bi-phase and Ca−Bi

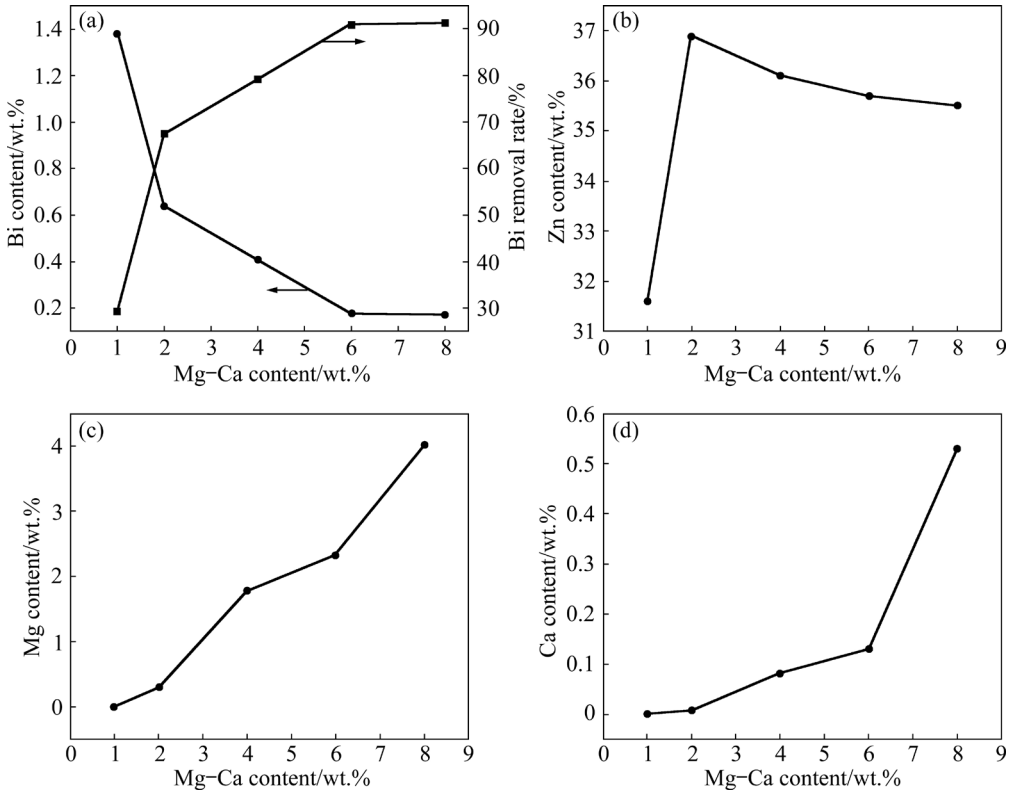

Fig. 9 Chemical compositions of brass samples refined at different Mg−Ca alloy contents: (a) Bi; (b) Zn; (c) Mg; (d) Ca

compound. As the Mg−Ca alloy content increased up to 8 wt.%, the contents of Mg and Ca elements within the alloy were higher, and only a small amount of fine Bi-rich phase could be observed. Additionally, it can be seen from Fig. 10(c) that the Bi-rich phase appeared to be significantly aggregated and was mainly distributed near the β-phase.

3.5 Phase composition of brass alloys and slag after refining

Figure 11 displays the XRD patterns of the brass alloy and slag after refining at 980 °C for 20 min. From Fig. 11(a), it can be found that the brass alloy was composed of $Cu_{0.64}Zn_{0.36}$, CuZn, and a small amount of Cu_2Mg. The Bi-phase was not detected, which may be due to the interaction of the Mg−Ca alloy with Bi to form the intermediate compounds, leading to a decrease in Bi content.

Figure 11(b) shows the XRD pattern of the slag in the crucible after refining. The slag composition included various types of metal oxides and Ca−Bi compounds, in which ZnO, MgO, CuO, CaO, and Bi_2O_3 originated from the oxidation of the metal produced during the melting process of the scrap brass. Furthermore, the $Ca_3Bi_8O_{15}$ phase was detected in the XRD pattern, which was speculated to be the complex compound ($3CaO{\cdot}4Bi_2O_3$) formed by CaO and Bi_2O_3. The presence of $CaBi_2$ and Ca_2Bi phases indicated that the Ca element reacted with the Bi element to form low-density Ca−Bi intermetallic compounds, which effectively decreased the Bi content in the scrap brass. The results of the XRD pattern were consistent with the above results.

4 Reaction mechanism

4.1 Thermodynamic calculation

In order to analyze the feasibility of the reaction between Mg−Ca alloys and Bi element, the thermodynamic calculation was performed using the thermodynamic software Factsage 8.2. The reaction temperature range was set to be 300−1300 °C with a temperature interval of 100 °C. The reaction module of Factsage 8.2 software was used to calculate the standard Gibbs free energy changes of oxidation reaction of metal element and the possible reactions between metal element in the scrap brass, as shown in Fig. 12. Tables 2 and 3 show the chemical equations for all possible reactions.

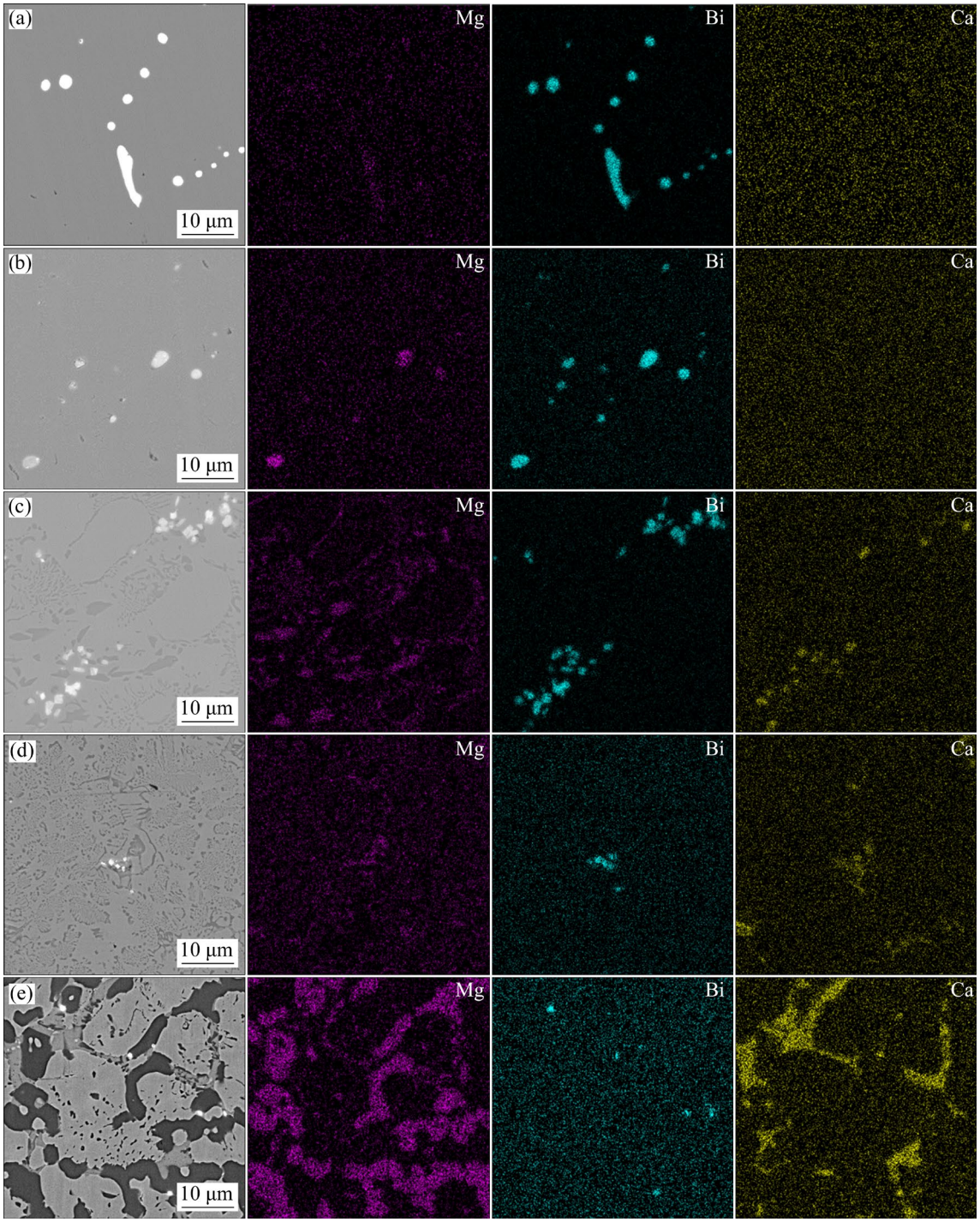

Fig. 10 SEM−EDS images of brass samples refined at different Mg−Ca alloy contents: (a) 1 wt.%; (b) 2 wt.%; (c) 4 wt.%; (d) 6 wt.%; (e) 8 wt.%

All the reaction equations had negative Gibbs free energy change, suggesting that the chemical reactions can proceed spontaneously in this temperature range. Among them, the Gibbs free energy change of Eq. (6) was the lowest, followed by Eqs. (5), (1) and (2). This result indicated that both Mg and Ca elements were easily oxidized compared to Zn and Bi elements. However, the highest Gibbs free energy change for the reaction of Cu with O_2 indicated that Cu element was the least susceptible to oxidation among all the reactions. In contrast, Cu_2O was relatively easy to form.

The lowest Gibbs free energy change of Eq. (7) indicated that Ca was most likely to react with Bi to form the Ca_3Bi_2 compound, followed by Eq. (8), and Mg also reacted readily with Bi to form the

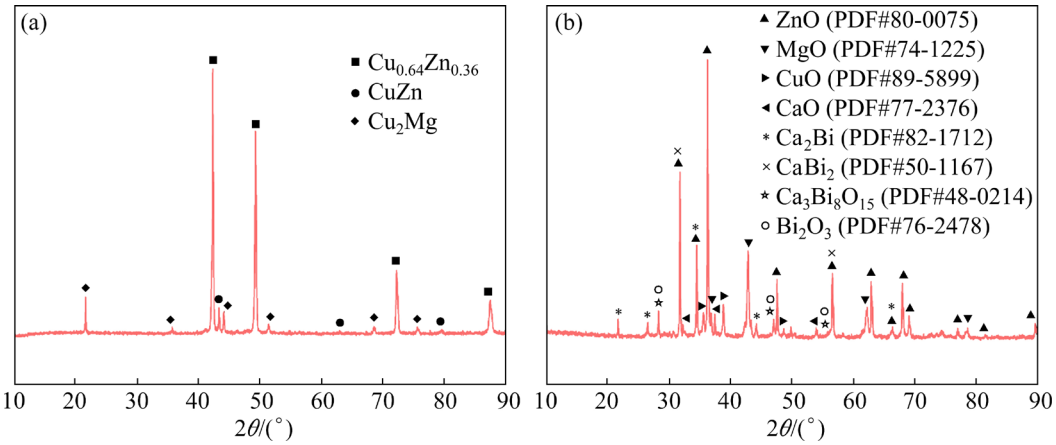

Fig. 11 XRD patterns of brass alloy (a) and slag (b) with Mg−Ca alloy content of 6 wt.% after refining at 980 °C for 20 min

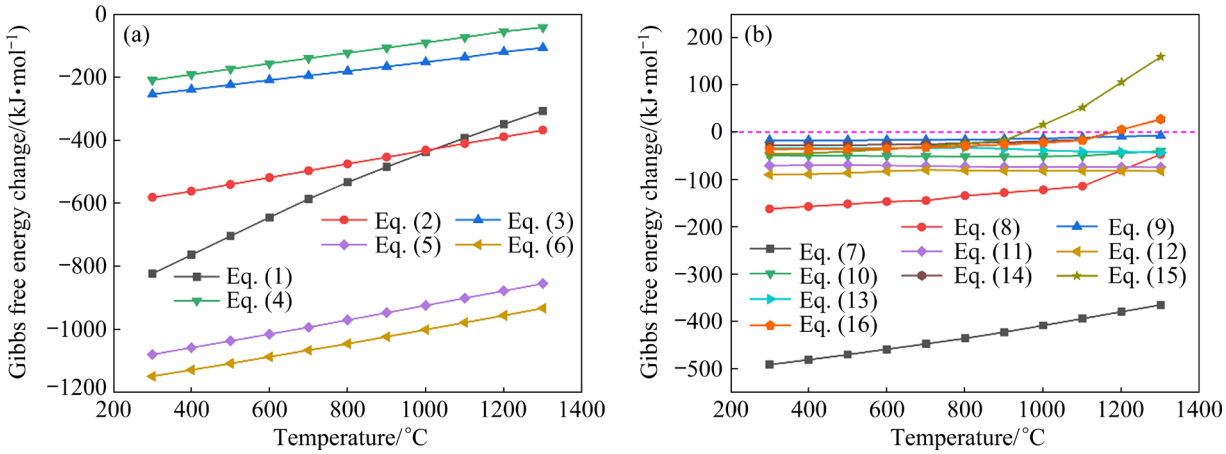

Fig. 12 Standard Gibbs free energy changes for all chemical reactions in Cu−Zn−Bi−Mg−Ca−O system

Table 2 Chemical equations for oxidation reactions of metal elements

Reaction	Equation
$4Bi+3O_2(g)=2Bi_2O_3$	(1)
$2Zn+O_2(g)=2ZnO$	(2)
$4Cu+O_2(g)=2Cu_2O$	(3)
$2Cu+O_2(g)=2CuO$	(4)
$2Mg+O_2(g)=2MgO$	(5)
$2Ca+O_2(g)=2CaO$	(6)

Table 3 Chemical equations for possible reactions of Ca and Mg elements with metal elements

Reaction	Equation
$3Ca+2Bi=Ca_3Bi_2$	(7)
$3Mg+2Bi=Mg_3Bi_2$	(8)
$2Ca+Cu=Ca_2Cu$	(9)
$Ca+5Cu=CaCu_5$	(10)
$Ca+Zn=CaZn$	(11)
$Ca+2Zn=CaZn_2$	(12)
$2Cu+Mg=Cu_2Mg$	(13)
$2Mg+Cu=Mg_2Cu$	(14)
$2Mg+3Zn=Mg_2Zn_3$	(15)
$2Mg+Ca=Mg_2Ca$	(16)

Mg_3Bi_2 compound. However, except for Eq. (15), the Gibbs free energy change values from Eq. (9) to Eq. (16) were not significant with increasing temperature, which are much higher than those for Eqs. (7) and (8). For Eq. (15), the Gibbs free energy change value was positive ($\Delta G>0$) when the temperature exceeded 950 °C, indicating that the reaction cannot proceed spontaneously.

In this study, from the thermodynamic point of view and combined with the above experimental results, the effects of melting temperature, holding

time, and Mg−Ca alloy content on the removal of the Bi element were as follows:

(1) The standard Gibbs free energy change value for the reaction between Ca and Bi element increased gradually with increasing temperature, indicating that high temperature was unfavorable for the reaction. In this experiment, the content of Bi element decreased as the melting temperature increased to 1000 °C, which was consistent with the results of thermodynamic calculation. However, when the melting temperature was increased to 1020 and 1040 °C, the content of Bi element decreased. Combined with the XRD results of slag (Fig. 11(b)), it can be found that the Bi element was likely to be oxidized and complexed with CaO to form the $Ca_3Bi_8O_{15}$ phase, resulting in a further decrease in the content of Bi element.

(2) When the holding time was increased from 0 to 20 min, the content of Bi element decreased from 0.77 wt.% to 0.178 wt.%, which indicated that the appropriate extension of the holding time could promote the Bi removal reaction and Ca−Bi compound floating. At this time, the small-sized slag had a tendency to grow up to a large size. When exceeding a certain holding time, the agglomerated large-sized slag tended to disperse, thus weakening the effect of NaF flux on the Ca−Bi compounds of the aggregation of slag, which decreased the Bi removal rate. However, when the holding time was extended to 40 min, the content of Bi element was reduced, which may be due to the long holding time, resulting in a part of Bi element being lost by oxidation.

(3) The content of Bi element decreased gradually with the increase of Mg−Ca alloy content. When the Mg−Ca alloy content was lower than 2 wt.%, the Bi-rich phase particles were composed of single Bi and Mg_3Bi_2 phase, which improved the hot working properties of brass alloy to some extent. With the Mg−Ca alloy content exceeding 4 wt.%, the Bi-rich phase particle was mainly composed of Ca−Bi compounds. The Bi content after refining did not change significantly when the content of Mg−Ca alloy was 6 wt.% and 8 wt.%, respectively, indicating that there was a certain limitation of the Bi removal reaction. The increase of Mg content simultaneously promoted the generation of β-phase and Cu_2Mg in the brass matrix, which was conducive to improving the cutting performance of brass alloy, but it greatly deteriorated the plasticity of recycled brass alloy. The Ca element was highly reactive, and it was oxidized to form CaO. On the one hand, Ca could react with the impurity Bi element to form Ca−Bi compounds, on the other hand, Ca can also form second phase particles with other elements in the brass matrix, which hindered the slagging of NaF flux and Ca−Bi compounds to a certain extent.

The thermodynamic calculation showed that both Ca and Mg elements were prone to react with Bi element to form Ca−Bi and Mg−Bi intermetallic compounds, which in turn changed the content and distribution morphology of Bi element in the brass.

4.2 Removal of Ca−Bi compound by flotation

The separation of Ca−Bi compounds in the scrap brass melt was affected by the mutual effect of the uplift force formed by the density difference and the viscous resistance of the brass melt. From Stokes' formula [31], the Ca−Bi compound will be subjected to the viscous force (P) and the buoyancy force (F) of the brass melt during the separation process, where P and F can be expressed by the following formula:

$$P=6\pi r v\eta \tag{17}$$

$$F=V(\rho_{\text{Brass}}-\rho_{\text{Ca-Bi}}) \tag{18}$$

where r is the equivalent radius of the Ca−Bi intermetallic compound, v is the uplift velocity of the Ca−Bi compound, η is the viscosity of the brass melt, V is the volume of the Ca−Bi intermetallic compound, ρ_{Brass} is the density of the brass melt, and $\rho_{\text{Ca-Bi}}$ is the density of the Ca−Bi intermetallic compound.

When the forces acting on the Ca−Bi intermetallic compound reach equilibrium, $P=F$, the uplift velocity (v) of the Ca−Bi compound was obtained as

$$v=\frac{V(\rho_{\text{Brass}}-\rho_{\text{Ca-Bi}})g}{6\pi r\eta} \tag{19}$$

where g is the acceleration of gravity.

Assuming that the Ca−Bi compounds are spherical particles, Eq. (19) can be further modified to

$$v=\frac{2r^2(\rho_{\text{Brass}}-\rho_{\text{Ca-Bi}})g}{9\eta} \tag{20}$$

Therefore, to obtain a sufficiently large uplift velocity for the Ca−Bi compounds, several

conditions must be satisfied: (1) the density of the compounds is less than that of the melt, (2) the viscosity of the melt is low, and (3) the particle size of the Ca−Bi compound is sufficiently large.

In this work, the densities of Ca−Bi intermetallic compounds [32] such as Ca_2Bi, $CaBi_2$, and CaBi are 5.21, 8.23, and 6.33 g/cm^3, respectively, which are smaller than the density of the brass melt (8.5 g/cm^3). Thus, the density difference provides a driving force for the uplift of Ca−Bi compounds.

Assuming that the surface tension (σ) of the brass melt is 1.35 N/m and the viscosity η is 4.38×10^{-3} Pa·s, the uplift velocity of the Ca−Bi compound can be obtained by substituting the above data into Eq. (20), as shown in Table 4. It can be seen that the uplift velocities of Ca_2Bi, $CaBi_2$, and CaBi compounds were 0.102, 0.098, and 0.101 mm/s, respectively, which verifies the feasibility of the uplift of Ca−Bi compounds from the kinetic point of view.

Table 4 Equivalent radius and uplift velocity of Ca−Bi compounds

Ca−Bi compound	r/mm	v/(mm·s^{-1})
Ca_2Bi	7.9×10^{-3}	0.102
$CaBi_2$	2.7×10^{-2}	0.098
CaBi	9.7×10^{-3}	0.101

In addition, fluid viscosity reflects the degree of resistance that a substance experiences as it moves through a fluid. The greater the viscosity is, the greater the resistance to flow is when the substance moves. The viscosity of NaF flux is 1.8×10^{-3} Pa·s [33], which is lower than the viscosity of copper melt (4.38×10^{-3} Pa·s) [34], and the addition of NaF flux to brass melt will decrease its melt viscosity and the resistance to the uplift of Ca−Bi compound will be reduced. Figure 13(a) shows the schematic diagram of the uplift of Ca−Bi compound. Combined with Eq. (20), it can be found that under the influence of the NaF flux, the Ca−Bi compound undergoes the agglomeration and complexation reactions to form a large-sized slag, which is prone to float to the melt surface, thus realizing the removal of Bi element.

4.3 Wetting and adsorption of NaF flux

The principle of melt purification is to purify the melt by adsorbing and dissolving inclusion and compound in the copper melt, and then removing them after floating to the surface of the copper melt via the density difference. The function of the flux can be divided into covering performance, separation performance, and slag removal performance. For the slag removal performance of the flux, the flux mainly relies on its adsorption wetting or immersion wetting to achieve the purpose of removing inclusions [35]. The type of flux wetting inclusions is determined by the size relationship between the radius (R) of the spherical crown of the molten salt and the size of the inclusions (L). When $2R<L$, the flux wets the inclusions by adhesion. When $2R>L$, the flux wets the inclusions by immersion. When the refining flux is added to the brass melt, the slag removal performance of the flux is determined by the extent of wetting between the flux and the inclusion, where the wetting angle of the flux on the inclusions is the key factor in determining its wetting performance.

Figure 13(b) shows the schematic diagram of NaF flux wetting and adsorption of the Ca−Bi compound. Setting the surface tension between the NaF flux and the brass melt as σ_{N-M}, the surface tension between the NaF flux and the Ca−Bi compounds as σ_{N-C}, the surface tension between the brass melt and the Ca−Bi compounds as σ_{M-C}, and the wetting angle between the flux and the Ca−Bi compounds as θ, σ_{N-M}, σ_{N-C}, and σ_{M-C} and θ satisfy the following relation [36]:

$$\sigma_{M-C} = \sigma_{N-C} + \sigma_{N-M}\cos\theta \tag{21}$$

$$\cos\theta = \frac{\sigma_{M-C} - \sigma_{N-C}}{\sigma_{N-M}} \tag{22}$$

In addition, the flux refining process of brass melt was mainly divided into three steps [37,38]: (1) the collision of the melt and inclusions during the convection of the melt; (2) the adsorption of inclusions by the flux; (3) the uplift of the agglomerates of inclusions and flux to the melt surface during the holding process. In the above process, the second step played a crucial role. The change in Gibbs free energy (ΔG_w) for wetting and adsorbing inclusions during the flux refining process can be derived from the following formula [38]:

$$\Delta G_w = [(\sigma_{N-C} + \sigma_{N-M}) - \sigma_{M-C}]\cdot\Delta\omega \tag{23}$$

where $\Delta\omega$ is the increment of interfacial area. The

results showed that decreasing σ_{N-M}, σ_{N-C} and increasing σ_{M-C} are beneficial to promoting flux wetting and adsorption of inclusions. According to the relevant literature [35,39], the addition of NaF flux can reduce the interfacial tension between it and the inclusion, thus decreasing the wetting angle between it and the inclusion. Therefore, by combining Formulas (22) and (23), it can be concluded that the addition of NaF flux can effectively wet and adsorb the Ca−Bi compound, i.e., the wettability between NaF flux and Ca−Bi compounds is better. From a thermodynamic perspective on flux wetting and adsorption, it can be explained why Ca−Bi compounds were prone to agglomerate and cause slag to float.

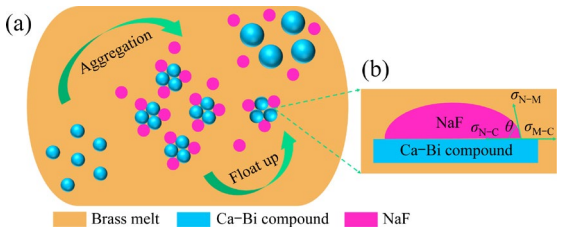

Fig. 13 Schematic diagrams of separation of Bi element: (a) Uplift of Ca−Bi compound; (b) NaF flux wetting and adsorption of Ca−Bi compound

5 Conclusions

(1) The thermodynamic calculation showed that both Mg and Ca elements were prone to form the Ca_3Bi_2 and Mg_3Bi_2 intermetallic compounds with the Bi element, which is favorable for the removal of Bi element.

(2) The optimal parameters were a melting temperature of 980 °C, a holding time of 20 min, and a Mg−Ca alloy content of 6 wt.%. The Bi element content can be decreased from 1.95 wt.% to 0.178 wt.% and the impurity removal rate reached 90.9%. Only a small amount of Bi-rich phase can be observed in the brass alloy after refining, and the brass matrix was obviously purified.

(3) NaF flux played a role in reducing viscosity because its viscosity was lower than that of the brass melt. The addition of NaF flux decreased the interfacial tension between it and the Ca−Bi compound. It can effectively wet and adsorb Ca−Bi compounds, thus prompting their agglomeration and uplift to the melt surface, and ultimately realizing the effective removal of the Bi element.

CRediT authorship contribution statement

Fei-ran JIANG: Methodology, Investigation, Formal analysis, Writing − Original draft, Review & editing; **Chuan-rong JIAO** and **Li-juan WANG:** Investigation, Formal analysis, Visualization; **Rui-lin WU:** Formal analysis, Visualization; **Yan-bin JIANG:** Conceptualization, Methodology, Resources, Writing − Review & editing; **Qian LEI:** Methodology, Writing − Review & editing; **Meng WANG:** Formal analysis, Visualization; **Zhu XIAO:** Methodology, Validation; **Zhou LI:** Writing − Review & editing.

Declaration of competing interest

The authors declare that they have no known competing financial interests or personal relationships that could have appeared to influence the work reported in this paper.

Acknowledgments

The authors acknowledge the financial supplies supported by the National Natural Science Foundation of China (Nos. U2202255, 52371038), and the Science and Technology Innovation Program of Hunan Province, China (No. 2023RC1019).

References

[1] LIU Shuo, ZHANG Yuan-bo, SU Zi-jian, LU Man-man, GU Fo-quan, LIU Ji-cheng, JIANG Tao. Recycling the domestic copper scrap to address the China's copper sustainability [J]. Journal of Materials Research and Technology, 2020, 9(3): 2846−2855.

[2] LIU Sen, LIU Wei, TAN Quan-yin, LI Jin-hui, QIN Wen-qing, YANG Cong-ren. The impact of China's import ban on global copper scrap flow network and the domestic copper sustainability [J]. Resources, Conservation and Recycling, 2021, 169: 105525.

[3] TIAN Hong-yu, GUO Zheng-qi, PAN Jian, ZHU De-qing, YANG Cong-cong, XUE Yu-xiao, LI Si-wei, WANG Ding-zheng. Comprehensive review on metallurgical recycling and cleaning of copper slag [J]. Resources Conservation and Recycling, 2021, 168: 105366.

[4] LIU Cheng-fei, LIU Da-fang, SHU Bo, XIA Hong-ying. Research progress on electrolytic refining technology of crude copper from scrap copper smelting [J]. Nonferrous Metals Engineering, 2024, 14(5): 1−17. (in Chinese)

[5] LI Li-quan, LIU Gong-qi, PAN De-an, WANG Wei, WU Yu-feng, ZUO Tie-yong. Overview of the recycling technology for copper-containing cables [J]. Resources, Conservation and Recycling, 2017, 126: 132−140.

[6] CAPUZZI S, TIMELLI G. Preparation and melting of scrap

in aluminum recycling: A review [J]. Metals, 2018, 8(4): 249.

[7] HSIEH C C, WANG J S, WU P T, WU W T. Microstructural development of brass alloys with various Bi and Pb additions [J]. Metals and Materials International, 2013, 19(6): 1173−1179.

[8] SCHULTHEISS F, JOHANSSON D, BUSHLYA V, ZHOU J M, NILSSON K, STÅHL J E. Comparative study on the machinability of lead-free brass [J]. Journal of Cleaner Production, 2017, 149: 366−377.

[9] ZHOU Bo, LIU Bo, ZHANG Shen-gen, LIN Rui, JIANG Yu, LAN Xue-ying. Microstructure evolution of recycled 7075 aluminum alloy and its mechanical and corrosion properties [J]. Journal of Alloys and Compounds, 2021, 879: 160407.

[10] LIN Rui, LIU Bo, ZHANG Jun-jie, ZHANG Shen-gen. Microstructure evolution and properties of 7075 aluminum alloy recycled from scrap aircraft aluminum alloys [J]. Journal of Materials Research and Technology, 2022, 19: 354−367.

[11] GAO Jian-wei, SHU Da, WANG Jun, SUN Bao-de. Effects of $Na_2B_4O_7$ on the elimination of iron from aluminum melt [J]. Scripta Materialia, 2007, 57(3): 197−200.

[12] GAO Jian-wei, SHU Da, WANG Jun, SUN Bao-de. Study on iron purification from aluminium melt by $Na_2B_4O_7$ flux [J]. Materials Science and Technology, 2009, 25(5): 619−624.

[13] GAO Jian-wei, SHU Da, WANG Jun, SUN Bao-de. Effect of boron on removal of iron from aluminium melts [J]. Materials Science and Technology, 2009, 25(12): 1462−1466.

[14] GAO Hong-tao, WU Guo-hua, DING Wen-jiang, LIU Liu-fa, ZENG Xiao-qin, ZHU Yan-ping. Study on Fe reduction in AZ91 melt by B_2O_3 [J]. Materials Science and Engineering: A, 2004, 368(1/2): 311−317.

[15] LI Hai-hong, SUN Xue-qin, ZHANG Shang-zhou, ZHAO Qin-yi, WANG Guang-zhen. Application of rare-earth element Y in refining impure copper [J]. International Journal of Minerals, Metallurgy, and Materials, 2015, 22(5): 453−459.

[16] WAN Bing-bing, CHEN Wei-ping, LIU Lu-sheng, GAO Xue-yang, ZHOU Li, FU Zhi-qiang. Effect of trace yttrium addition on the microstructure and tensile properties of recycled Al−7Si−0.3Mg−1.0Fe casting alloys [J]. Materials Science and Engineering: A, 2016, 666: 165−175.

[17] SONG Dong-fu, ZHAO Yu-liang, JIA Yi-wang, LI Xin-tao, FU Ya-nan, ZHANG Wei-wen. Synergistic effects of Mn and B on iron-rich intermetallic modification of recycled Al alloy [J]. Journal of Materials Research and Technology, 2023, 24: 527−541.

[18] LI Xiang, MA Bao-zhong, WANG Cheng-yan, CHEN Yong-qiang. Microstructure evolution and ductility improvement mechanism of Fe-containing recycled brass alloy after Mn addition [J]. Materials Chemistry and Physics, 2024, 313: 128724.

[19] LIU Wei, MA Bao-zhong, ZHOU Zhen-gen, ZUO Yi-chang, WANG Ling, CHEN Yong-qiang, WANG Cheng-yan. Efficient separation of impurities in scrap copper by sulfurization-vacuum distillation [J]. Vacuum, 2022, 202: 111145.

[20] NAKANO A, KAJIYA N, YAMADA K, NAKAMURA S I, MATSUDA T, SUEYOSHI H. Removal of lead from scrap bronze [J]. Materials Transactions, 2006, 47(12): 2997−3000.

[21] HILGENDORF S, BINZ F, WELTER J M, FRIEDRICH B. Lead removal from brass scrap by fluorine-free compound separation [J]. Materials Science and Technology, 2016, 32(17): 1782−1788.

[22] NAKANO A, ROCHMAN N T, SUEYOSHI H. Removal of lead from copper alloy scraps by compound-separation method [J]. Materials Transactions, 2005, 46(12): 2719−2724.

[23] ZHANG Bao-yu, HUANG Xiao-shan, ZHANG Xin-fang, MA Bao-zhong, WANG Cheng-yan. Purification of Cu−Zn melt based on the migration behavior of lead and bismuth under pulsed electric current [J]. Journal of Cleaner Production, 2023, 396: 136577.

[24] HUANG Xiao-shan, ZHAO Hong-liang, WANG Cheng-yan, ZHANG Xin-fang. One-step separation of hazardous element lead in brass alloy by physical external field [J]. Journal of Cleaner Production, 2020, 276: 123358.

[25] SUN Ya-min, HUANG Xiao-shan, LIU Chang-hao, ZHOU Meng-cheng, ZHANG Xin-fang. Impurity iron separation from molten secondary aluminum by pulsed electric current [J]. Journal of Alloys and Compounds, 2023, 934: 167903.

[26] LUO Kun, WANG Zhe, MENG Long, GUO Zhan-cheng. Removal of iron for aluminum recovery from scrap aluminum alloy by supergravity separation with manganese addition [J]. Chemical Engineering and Processing—Process Intensification, 2022, 173: 108841.

[27] LI Hang, NIU Dong-tao, ZHANG Zhong-tao, YANG Fan, WANG Hong-xia, CHENG Wei-li. Tailoring microstructure, mechanical and wear properties of Mn_5Si_3 reinforced Cu−35Zn−3Al alloy via melt superheat combined with pulsed magnetic field [J]. Transactions of Nonferrous Metals Society of China, 2024, 34(3): 918−934.

[28] LU Dian-kun, JIN Zhe-nan, CHANG Yong-feng, SUN Shu-chen. Mechanism of debismuthizing with calcium and magnesium [J]. Transactions of Nonferrous Metals Society of China, 2013, 23(5): 1501−1505.

[29] ADINEH M, DOOSTMOHAMMADI H. Microstructure, mechanical properties and machinability of Cu−Zn−Mg and Cu−Zn−Sb brass alloys [J]. Materials Science and Technology, 2019, 35(12): 1504−1514.

[30] ZHU Quan-li, WU Wei-dong, LIU Kai-zhou, CHEN Geng-chun, CHEN Wei-ping. Study on microstructure and properties of brass containing Sb and Mg [J]. Science in China Series E: Technological Sciences, 2009, 52(8): 2172−2174.

[31] QIAN Ma, ZHENG Li-hui, GRAHAM D, FROST M T, STJOHN D H. Settling of undissolved zirconium particles in pure magnesium melts [J]. Journal of Light Metals, 2001, 1(3): 157−165.

[32] NOTIN M, MEJBAR J, BOUHAJIB A, CHARLES J, HERTZ J. The thermodynamic properties of calcium intermetallic compounds [J]. Journal of Alloys and Compounds, 1995, 220(1/2): 62−75.

[33] HAN Ming-rong, ZHANG Sheng-qin. Principles of metallurgy [M]. Beijing: Metallurgical Industry Press, 2008. (in Chinese)

[34] LIU Chun-peng. Physical chemistry of copper metallurgy

[M]. Shanghai: Shanghai Science and Technology Press, 1990. (in Chinese)
[35] LI Cong, LI Jian-guo, MAO Yi-zhe, JI Jia-cheng. Mechanism to remove oxide inclusions from molten aluminum by solid fluxes refining method [J]. China Foundry, 2017, 14(4): 233−243.
[36] WAN Bing-bing, LI Wen-fang, LIU Fang-fang, LU Ti-wen, JIN Shuo-xun, WANG Kang, YI Ai-hua, TIAN Jun, CHEN Wei-ping. Determination of fluoride component in the multifunctional refining flux used for recycling aluminum scrap [J]. Journal of Materials Research and Technology, 2020, 9(3): 3447−3459.
[37] WANG Wei, WU Guo-hua, SUN Ming, HUANG Yu-guang, WANG Qu-dong, DING Wen-jiang. Effects of flux containing YCl3 on the yttrium loss, mechanical and corrosion properties of Mg−10Gd−3Y−0.5Zr alloy [J]. Materials Science and Engineering: A, 2010, 527(6): 1510−1515.
[38] TONG Xin, WU Guo-hua, SUN Ming, WANG Qi-man, ZHANG Liang, LIU Wen-cai. Realizing the purification and grain refinement of Mg−Gd−Y alloy by one-step flux refining [J]. Journal of Materials Science & Technology, 2024, 173: 202−217.
[39] SHI Ming, LI Ying. Performance improvement in aluminum alloy treated by salt flux with different fluorides [J]. Journal of Materials Engineering and Performance, 2023, 32(7): 3065−3072.

复合分离法高效去除废杂黄铜中的杂质 Bi 元素

姜斐然[1]，焦传熔[1]，王丽娟[1]，武瑞麟[1]，姜雁斌[1,2,3]，雷 前[2]，王 檬[1]，肖 柱[1,3]，李 周[1,2,3]

1. 中南大学 材料科学与工程学院，长沙 410083；
2. 中南大学 粉末冶金国家重点实验室，长沙 410083；
3. 铜基新材料山西省重点实验室，运城 044000

摘 要：高效去除废杂黄铜中的杂质 Bi 元素可促进黄铜的回收再利用。采用复合分离法，研究了熔炼温度、保温时间和 Mg−Ca 合金含量对杂质 Bi 元素去除效果的影响。从热力学角度揭示了复合分离法去除 Bi 元素的机理。研究结果表明，在熔炼温度为 980 ℃、保温时间为 20 min 以及 Mg−Ca 合金含量为 6% (质量分数)的最佳工艺参数条件下，杂质 Bi 含量由 1.95% (质量分数)降低至 0.178% (质量分数)，除杂率达到 90.9%。精炼后黄铜基体内还残留少量的 Ca−Bi 化合物。NaF 熔剂因其黏度低和具有降低表面张力的作用而能有效地润湿和吸附 Ca−Bi 化合物，促进 Ca−Bi 化合物团聚和上浮至熔体表面，从而确保 Bi 元素的充分去除。

关键词：废杂黄铜；富 Bi 相；Mg−Ca 合金化；复合分离法

(Edited by Wei-ping CHEN)